‘Fraternal-twin’ ferroelectricity: competing polar states in hydrogen-doped samarium nickelate from first principles

OPEN ACCESS
IOP Publishing
Journal of Physics: Condensed Matter
J. Phys.: Condens. Matter **36** (2024) 355603 (7pp)
https://doi.org/10.1088/1361-648X/ad5091

'Fraternal-twin' ferroelectricity: competing polar states in hydrogen-doped samarium nickelate from first principles

Michele Kotiuga[1,3,*] **and Karin M Rabe**[2]

[1] Theory and Simulation of Materials (THEOS), École Polytechnique Fédérale de Lausanne, CH-1015 Lausanne, Switzerland
[2] Department of Physics and Astronomy, Rutgers, The State University of New Jersey, Piscataway, NJ 08854, United States of America

E-mail: michele.kotiuga@epfl.ch

Received 26 February 2024, revised 23 April 2024
Accepted for publication 24 May 2024
Published 7 June 2024

Abstract

In ferroelectric switching, an applied electric field switches the system between two polar symmetry-equivalent states. In this work, we use first-principles calculations to explore the polar states of hydrogen-doped samarium nickelate (SNO) at a concentration of 1/4 hydrogen per Ni. The inherent tilt pattern of SNO and the presence of the interstitial hydrogen present an insurmountable energy barrier to switch these polar states to their symmetry-equivalent states under inversion. We find a sufficiently low barrier to move the localized electron to a neighboring NiO_6 octahedron, a state unrelated by symmetry but equal in energy under a square epitaxial strain ($a = b$), resulting in a large change in polarization. We term this unconventional ferroelectric a 'fraternal-twin' ferroelectric.

Supplementary material for this article is available online

Keywords: ferroelectricty, rare-earth nickelates, charge localization

1. Introduction

In the prototypical perovskite oxide ferroelectrics, a soft polar mode gives rise to symmetry-equivalent insulating polar states that can be switched by an applied electric field [1]. For many years these systems have been studied alongside hydrogen-bonded ferroelectrics, such as Rochelle salt and KH_2PO_4, the first class of ferroelectrics to be discovered [2, 3]. In recent years, in part motivated by the search for ferromagnetic-ferroelectric multiferroics, there has been great interest in the design and discovery of ferroelectrics with alternative mechanisms. Examples include improper ferroelectrics, driven by a single non-polar mode that couples to the polar mode at higher order ($YMnO_3$ [4]), hybrid improper ferroelectrics, involving the combination of multiple non-polar distortions ($Ca_3Mn_2O_7$ [5]); and charge ordering of multiple valence states [6], such as the iron in magnetite [7]. Superlattice ordering has been explored as a means to break selected symmetries to activate relevant nonlinear couplings or to make a particular ordering polar [8, 9]. In each case,

[3] Current address: Materials Design SARL, 92120 Montrouge, France.
[*] Author to whom any correspondence should be addressed.

multiple symmetry-equivalent insulating polar states at the same energy are separated by barriers surmountable by accessible electric fields.

Recent experimental work has shown that samarium nickelate, $SmNiO_3$ (SNO) can be electron-doped by the reversible intercalation of hydrogen or lithium. Both experimental measurements and first-principles calculations show that the valence electrons of the intercalant localize on NiO_6 octahedra, changing the nominal valence of the Ni from 3+ to 2+, with the system remaining insulating for intercalant concentrations up to one per Ni [10–13]. First-principles calculations show that the favored sites for the intercalant ions are interstitial sites outside the NiO_6 octahedra, with a spatial separation between the localized electron and the positively charged intercalant [11, 13]. Further, within the oxygen octahedron rotation pattern stabilized in the orthorhombic structure of undoped SNO, there are multiple choices of sites for the interstitial and corresponding choices for the NiO_6 octahedron to which the electron is added, yielding a large number of states comparable in total energy.

In this work, we systematically investigate low-energy states of hydrogen-doped SNO ($H_{1/4}SmNiO_3$) using first-principles calculations. The localization of the hydrogen valence electron on a nearby NiO_6 octahedron results in a local dipole pointing from the NiO_6 octahedron to the H^+ ion. These dipoles can be ordered to yield low-energy states with a net polarization. Due to the underlying oxygen-octahedron tilt pattern that strongly stabilizes the orthorhombic structure of undoped SNO, a large energy barrier between symmetry-equivalent polarization states prevents conventional ferroelectric switching. By applying in-plane square epitaxial strain (i.e. $a = b$) to tune the potential energy landscape, we can equalize the energy of two states with roughly opposite polarization and the same octahedron-rotation pattern, switching the position of the localized electron from one NiO_6 octahedron to a neighboring one. This system marries different symmetry-breaking aspects of charge-ordered ferroelectricity in oxides and hydrogen-bonded ferroelectrics along side a strain constraint leading to a switching that occurs between two states unrelated by symmetry, we refer to this as 'fraternal-twin ferroelectricity.'

2. Methods

Our first-principles DFT + U calculations are carried out using the Perdew–Burke–Enzerhof (PBE) functional [14, 15] as implemented in VASP [16, 17] with an energy cutoff of 520 eV and the Sm_3, Ni_pv, O, and H projector augmented wave (PAW) [18] potentials provided with the VASP package. The Sm_3 PAW potential includes the f-electrons in the core. We include a Hubbard U (within the rotationally invariant method of Liechtenstein *et al* [19]) with $U = 4.6$ eV and $J = 0.6$ eV following our previous work [13]. A 20-atom unit cell of SNO was used to accommodate the $a^-a^-c^+$ tilt pattern. We choose a G-type antiferromagnetic (AFM) ordering in our spin-polarized DFT calculations as our previous work has shown that the type of AFM ordering only affects the band width, but not the electron localization with electron doping. As SNO is paramagnetic in the temperature range of interest for ferroelectric properties, we do not study a ferromagnetic ordering. All structural relaxations were carried out with Gaussian smearing with $\sigma = 0.1$ eV (an appropriate value given the band gap of the material, see supplementary data section I) and a Monkhorst-Pack k-mesh of $6 \times 6 \times 4$ such that the forces were less than 0.005 eV Å^{-1}, with lattice constants $a = 5.278$ Å, $b = 5.818$ Å, $c = 7.421$ Å computed for undoped SNO. The density of states calculations were performed using the tetrahedral method with Blöchl corrections [20]. The projected density of states (PDOS) plots were generated using a Γ-centered k-point mesh and the site projected scheme of pymatgen [21]. The polarization was calculated using the Berry phase method, as implemented in VASP [22]. The branch choice was made such that the polarization aligned with the local dipole. The effects of epitaxial strain are studied with the strained-bulk method [23], with in-place lattice parameters $a = b$ fixed while the c-axis is allowed to relax. For the associated data, see the repository [24] hosted on the Materials Cloud [25].

We begin by calculating the relative energetics of adding a hydrogen atom at various candidate interstitial sites with corresponding choices for the location of the added electron. Specifically, in a $\sqrt{2} \times \sqrt{2} \times 2$ supercell of bulk SNO, we place one hydrogen atom in the plane bisecting the Ni-O-Ni bonds at the O for both apical and basal O sites, ±1 Å away from the O along the crystallographic axes. Subsequently, the valence electron localizes in one of the two octahedra that include the O. We allow the internal coordinates to relax while fixing the lattice parameters. The fixed lattice parameters allows us to compare the energetics of a number of structures and choose which ones to study further with epitaxial strain. Epitaxial strain in the (001) plane is applied in the strained-bulk method to tune the relative energies of the various configurations.

3. Results

Figure 1 shows the crystal structure of bulk SNO, figure 1(a), and the four of the lowest-energy structures identified for $H_{1/4}SNO$, (figures 1(b)–(e) and table 1), all of which are polar (see supplementary data, section II) for more structures). If the octahedron-rotation distortions were not present, these four configurations would be symmetry equivalent, with a local dipole pointing from the electron on the NiO_6 to the adjacent H^+ interstitial. The polarizations and relative energetics of the structures pictured in figures 1(b)–(e) are summarized in table 1. The polarization primarily arises from the separation of the hydrogen ion and its valence electron. As this separation is governed by the chemical bond formed between the hydrogen and nearby oxygen as well as the Ni–O hybridization, the values for the different structures are quite similar, though not identical. The differences in energy stem from the underlying tilt pattern of SNO. The hydrogen can be placed between two NiO_6 octahedra with an in-phase tilt along the $c-$axis (figure 1(b)) or an out-of-phase tilt along the $a-$ or

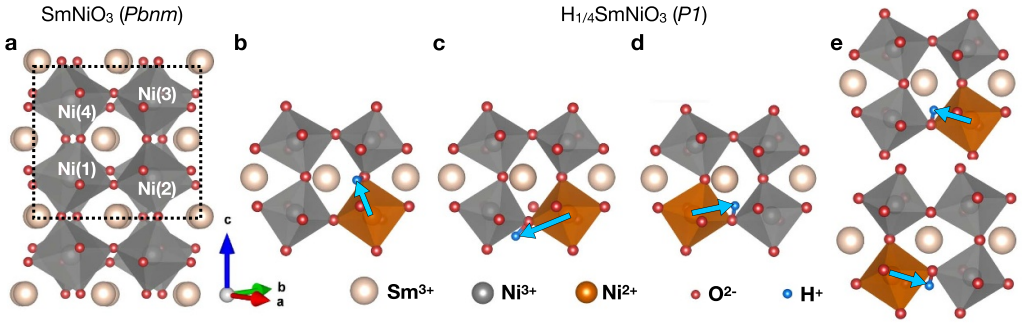

Figure 1. (a) Bulk $SmNiO_3$ (SNO) with the space group *Pbnm* (i.e. with an $a^-a^-c^+$ tilt pattern. The dashed box denotes the 20 atom unitcell with four nickel sites. (b)–(e) Four example structures of $H_{1/4}SmNiO_3$, i.e. one hydrogen added to the 20 atom unitcell, with the hydrogen bound to a basal or apical oxygen (relative to the *c*-axis). The hydrogen binds to an oxygen and its valence electron localizes on a nearby NiO_6 octahedron, colored orange. This results in a local dipole indicated by the cyan arrow. (e) The two 'identical twin' structures related by inversion.

Table 1. Relative energetics of relaxed $H_{1/4}SmNiO_3$ constrained to the lattice parameters of bulk $SmNiO_3$, $a = 5.278$ Å, $b = 5.818$ Å, $c = 7.421$ Å, a $\sqrt{2} \times \sqrt{2} \times 2$ supercell relative to the 5-atom primitive perovskite cell. The zero is set to be the low energy configuration, shown in figure 1(e).

H^+ between	Figure	Ni^{2+} (site)	Polarization ($\mu C\,cm^{-2}$)	Energy (meV/Ni)
Ni(2)&Ni(3)	Figure 1(b)	2	$34 = \lvert 24, -17, 17 \rvert$	55
Ni(1)&Ni(2)	Figure 1(c)	2	$31 = \lvert -10, -12, -26 \rvert$	26
Ni(1)&Ni(2)	Figure 1(d)	1	$28 = \lvert 6, 6, 26 \rvert$	24
Ni(1)&Ni(2)	Figure 1(e)	2	$30 = \lvert -7, -14, 25 \rvert$	0

b−axes (figures 1(c)–(e)). Placing the hydrogen between two NiO_6 octahedra with a relative out-of-phase tilt results in a lower energy. Furthermore, the in-phase tilts along the *c*−axis introduce a canting such that the energy is lowest when the hydrogen is placed above the basal oxygen (figure 1(e), upper). Finally, the orthorhombicity of the cell results in different energies for the two structures shown in figures 1(d) and (e), which are related by an electron hop from Ni(1) to Ni(2) with a similar position of the H^+.

For the lowest energy configuration, shown in figure 1(e), we also show the variant generated by inversion symmetry. We can see that switching between these two structures would involve either an electron hop from one NiO_6 to another accompanied by a complete reversal of the octahedron-rotation pattern, or a large-scale displacement of the interstitial H^+ ion from one side of the octahedron to the other, see supplementary data, section III for energy barrier.

We find that these hydrogen-doped states are all insulating, with similar electronic structures. In figure 2(b), we show the spin-polarized DOS of the lowest energy state (figure 1(e)). As in the spin-polarized DOS of undoped SNO, shown as a reference in figure 2(a), the computed gap is less than 1 eV. In the vicinity of the Fermi energy, the states are dominated by O 2*p* and Ni 3*d*. In particular, the unoccupied states are Ni e_g states hybridized with O-2*p* states. In the undoped case, there are three unoccupied states per nickel. Each nickel has a magnetic moment close to 1 μ_B, suggesting low-spin Ni^{3+}. Due to the strong hybridization with the O-2*p* states, we associate these states with the entire NiO_6 octahedron and to write the electronic configuration as $d^8\underline{L}$, i.e. d^8 with an oxygen ligand-hole. The added hydrogen results in the decrease in the number of unoccupied states from 4 to 3 in the feature closest to the Fermi energy. The spin-down Ni-3*d*/O-2*p* state associated with Ni(2) is moved to the top of the valence band and, dominated by oxygen, essentially fills the oxygen ligand-hole. The remaining unoccupied state associated with Ni(2), shown in orange, is pushed up in energy. The splitting of the lobes comes from the lowering of symmetry in these structures; however, as the electronic structure of the Ni^{3+} sites is nearly unchanged, the change in the band gap relative to the undoped case is negligible.

For ferroelectricity, we require two states with different polarization at the same energy with a low barrier for switching. Here, the state related to the ground state by an electron hop, without other major structural rearrangements, is 24 meV per Ni higher in energy. Application of an epitaxial strain constraint offers the possibility of tuning the relative energy of these two states. In figures 3(a)–(d), we show the effect of cubic epitaxial strain on the structures of figures 1(d) and (e), which we refer to as structure 1 and 2, respectively. The two structures appear quite similar, the essential difference being that the expanded octahedron contains Ni(1) or Ni(2) in the case of structure 1 and 2, respectively. The octahedron containing the localized electron is larger in volume by approximately 12% compared to the other octahedra, which are all roughly the same volume. The larger octahedron is also a bit distorted such that the longest bond is the Ni–O bond with the O on the side of the octahedron opposite to that of the H. For an analysis of all the structures found in figure 1 see supplementary data, figure 7. Figure 3(a) shows that the total energy curves as a function of in-plane lattice parameter. The total energy curves of these two structures cross near their respective minima at $a = 3.94$ Å, the calculated lattice constant for $SrTiO_3$ with DFT-PBE. This crossing can be more clearly seen in figure 3(b), which shows the difference of these two energy curves. Due to the epitaxial constraint, this crossing

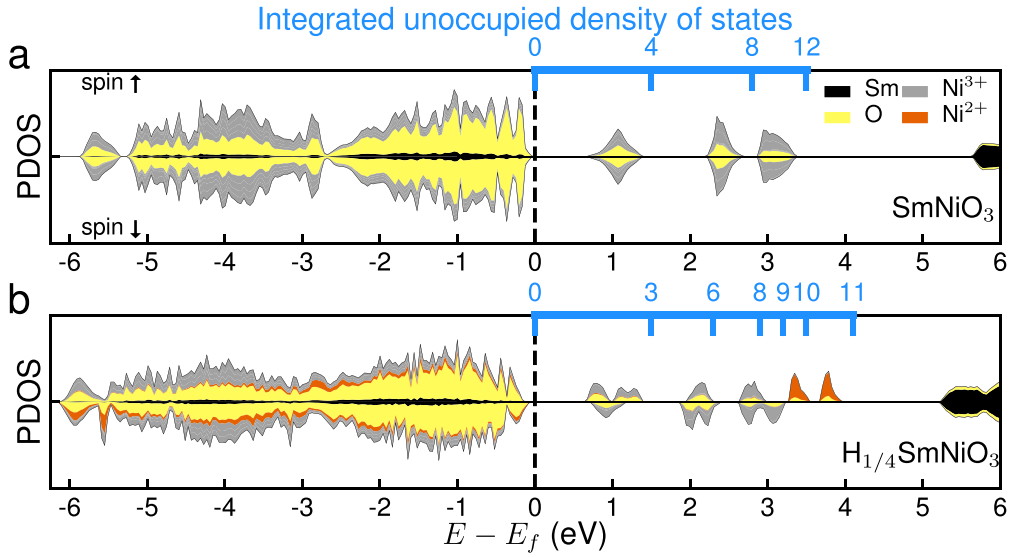

Figure 2. Spin-polarized PDOS for (a) SNO and (b) $H_{1/4}$SNO (figure 1(e)) for an AFM G-type magnetic ordering. The integrated unoccupied DOS is displayed along the top axis for $E - E_f \in [0,4]$. The element specific PDOS is shown in black for Sm, yellow for O, gray for Ni^{3+} and orange for Ni^{2+}.

occurs at an energy 70 meV/Ni higher than structure 2 with the bulk lattice parameters of SNO. Moreover for all values of a, the relaxed c-axis for the two structures is very close (within 0.02 Å), as shown in figure 3(c). Furthermore under an in-plane tensile strain the c-axis compresses, while the cell volume increases, as shown in figure 3(d). We note that at the bulk lattice parameters of SNO and $a > 3.86$ Å the OH bond is parallel to the c-axis, but for $a < 3.86$ Å the low energy position of the hydrogen atom changes and the OH bond lies in the ab-plane. For clarity, the latter structures are reported in the supplementary data, figure 9 and not included in figure 3.

To characterize the switching, we linearly interpolate between the structures 1 and 2 with $a = b = 3.94$ Å shown in figure 3(e). This is done by first identifying the change in position of each Sm, O and Ni atom from structure 1 to structure 2 and linearly interpolating between these two positions to generate 9 intermediate structures along a switching path. In other words for each atom its position for structure n is $\vec{x}_n = \vec{x}_i + \frac{n}{10}(\vec{x}_f - \vec{x}_i)$ where $\vec{x}_{i,f}$ is the position of the atom in the initial and final structures, respectively. For each of the structures along the interpolated switching path the positions of the Ni, O and Sm atom are kept fixed while the position of the H^+ ion is allowed to relax so that it remains at an energetically favorable site, while the rest of the cell is kept fixed with $a = b = 3.94$ Å and $c = 7.52$ Å. If one of the octahedra is larger than the others, the valence electron of the H will localize on the larger octahedron. In order to study the case where the two octahedra containing Ni(1) and Ni(2) are of equal volume we carried out two calculations: one with a higher initial moment on Ni(1) and the other with a higher initial moment on Ni(2). Results for the energy of states along the path, shown in figure 3(f), give an energy barrier of ∼50 meV/Ni, corresponding to a coercive field on the order of 300 kV cm^{-1}. Through this switching path, the system remains insulating, with the band gap shown in figure 3(f). We can clearly track the position of the localized added electron through the Ni magnetic moments. In figure 3(g) we observe a discrete jump, signifying that the electron hops from one NiO_6 octahedron to the other. At the midpoint of this path, the added electron can localize either on the octahedron containing Ni(1) or the one containing Ni(2), with a small energy difference due to the fact that the two states are not symmetry equivalent. Finally, in figure 3(h), we track the polarization in each Cartesian component through this switching path. P_z remains constant because the valence electron is hopping in the ab-plane, but we see a reversal of the polarization in the ab-plane, resulting in a sizable change in the polarization, $\Delta P = 27\mu$C cm^{-2}.

4. Discussion

This energy barrier in this system is much lower than is typical of a charge-ordered ferroelectric, where strong coupling between the structure and the charge ordering tends to lock the hopping charge into a particular site [26]. In this system, the $Ni^{3+}O_6$ octahedra surrounding the $Ni^{2+}O_6$ octahedron reduce the degree of structural relaxation, and the strong hybridization between the Ni and O states aids the electron hop, resulting in a lower lattice coupling and barrier. Despite this lower lattice coupling, the electron hop is nevertheless inextricably tied to the expanded volume of the NiO_6 octahedron it is localized on.

The ferroelectricity observed in this system depends on the long-range ordering of the local dipoles formed by the localized electron and the H^+ ion. The preferred binding location of the H^+ ion dictates and reduces the possible more complex long-range orderings, see figure 4. By doubling the supercell along the a and c pseudocubic directions, we can calculate the energy of non-polar structures where the orientation of the localized dipoles leads to no net polarization, figures 4(b)

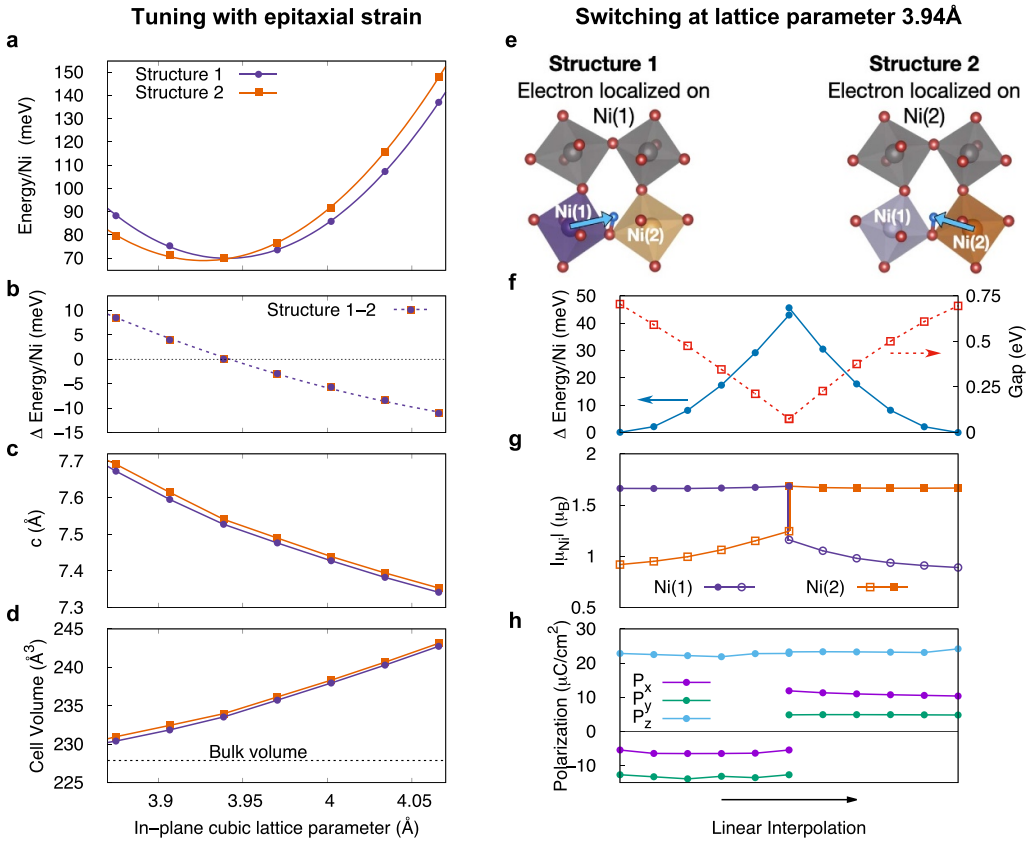

Figure 3. (a)–(d) The change in total energy and cell parameter as a function of in-plane epitaxial strain. (a) Total energy per nickel site as a function of the in-plane cubic lattice parameter for $H_{1/4}SNO$ with the hydrogen valence electron localized on the octahedra containing Ni(1) (purple circles), (a) left, and Ni(2) (orange squares), (a) left, with quadratic fits. The zero is set to the lowest energy configuration with the bulk lattice constants of SNO given in table 1. (b) The energy difference per nickel site for the electron localized on the octahedron containing Ni(1) or Ni(2) as a function of the in-plane lattice parameter. The solid line is the difference in the quadratic fits from panel (b). The relaxed *c*-lattice parameter, (c), and cell volume (d), as a function of the in-plane lattice parameter for the electron localized on the octahedra Ni(1) & (2). The lines serve only as a guide for the eye. The bulk cell volume, 227.9 $Å^3$, is indicated with the dashed black line. (e) Unit cell of structures 1, figure 1(d), and 2, figure 1(e), omitting the Sm atoms. (f)–(h) The change in properties along the linearly-interpolated switching path at an in-plane cubic lattice parameter of 3.94 Å. Details of the intermediate structures in the main text. (f) Change in total energy along the linearly interpolated switching path. (g) Magnetic moment of Ni(1), purple, and Ni(2), orange, along the switching path. (h) The polarization along each Cartesian component through the switching path.

and (c), as well as structures where the polarization is purely along the *c* and *a* pseudocubic directions, figures 4(d) and (e), respectively.) We find that the energies of the non-polar structures are slightly higher than the energy of our original structures. As the structure with the net polarization along the *c* axis is a 1:1 patterning of our two original equal-energy structures, figure 3(e), it is unsurprising that these three structures are comparable in energy. Further, we find that the structure with the net polarization along the *a* axis is 31 meV/Ni lower in energy, resulting in an energy difference of 35 meV/Ni between the lowest polar structure and the lowest non-polar structure. Since the electron hops within the *ab* plane, the net polarization along the *a* axis is expected to be switchable. This suggests that even though the ferroelectric switching may be more complicated than that suggested by figures 3(f)–(h), we expect to observe a switchable ferroelectric state.

Previous experimental work on electron-doped SNO suggests that this ferroelectric switching could be realized in the laboratory. Hysteresis at low biases has been observed in SNO on silicon [27]. It has been attributed to oxygen vacancies present in the system which effectively electron dope the system. Growing epitaxially-strained (001) SNO on $SrTiO_3$ applies the necessary strain to tune symmetry-inequivalent minima with very different polarizations to the same energy. The key will be to achieve a nearly homogeneous doping concentration throughout the thin film. As the intercalant mobility is dependent on temperature [28], we expect the change in polarization to be more robust at lower temperatures. Furthermore, the magnitude of the field should be chosen with care as it has been shown that in oxygen-deficient $NdNiO_3$ (NNO), the oxygen vacancies can be concentrated using an applied field [29] and in hydrogen-doped NNO and SNO on fluorine-doped tin oxide and indium tin oxide the H^+ distribution can be modulated with high speed electrical pulses [30]. Recently, studies of hydrogen-doped NNO have exhibited a remnant polarization that, at room temperature, decays on the order of one second highlighting the sensitivity of such a phenomenon to temperature and other external factors [31].

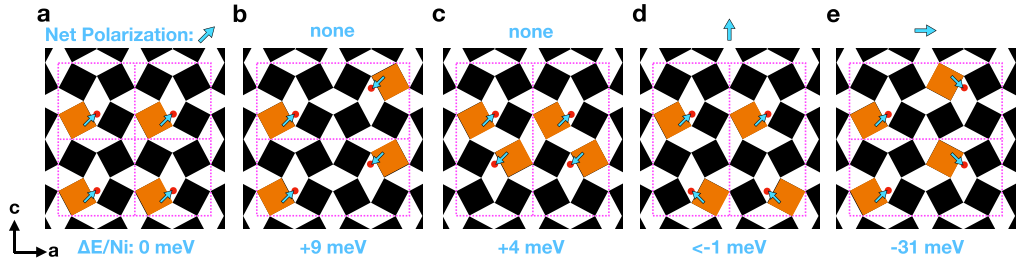

Figure 4. The *ac* plane of a number of orderings of the localized dipoles leading to various net polarizations. As the *ab* plane is constrained to cubic STO, considering ordering in the *bc* plane would yield equivalent structures. The black and orange squares represent $Ni^{3+}O_6$ and $Ni^{2+}O_6$ octahedra, respectively. The H^+ ion is indicated by the red circles, the localized dipole by the blue arrow, and the dashed pink box indicates the unitcell of the particular ordering. (a) Structure 1 constrained to the lattice parameter of $SrTiO_3$ (figure 3(e)—left) used as the reference energy. (b) and (c) Orderings in supercells doubled along the pseudocubic *a* and *c* directions, respectively, that have no net polarization and are slightly higher in energy than the reference structure. (d) Ordering in a supercell doubled along the pseudocubic *c* direction with a net polarization along the *c* axis only, which is approximately equal in energy to the reference structure and not switchable. (e) Ordering in a supercell doubled along the pseudocubic *a* direction with a net polarization along the *a* axis that is the lowest energy state found in these supercells.

As the two structures are not symmetry equivalent, we refer to this type of ferroelectricity by the term 'fraternal-twin.' The potential for fraternal-twin ferroelectricity in hydrogen-doped SNO arises from the rich configuration space of structures generated by the many inequivalent sites for the interstitial H^+ ion and its localized valence electron. In general, a polar structure does not ensure ferroelectricity as characteristics such as the tilt pattern or charge ordering can result in a insurmountable barrier to switching to the symmetry-related state. Fraternal-twin ferroelectricity provides an alternative mechanism for change in polarization with an electric field in materials when conventional ferroelectricity is thwarted by high energy barriers. Materials with a number of local minima close in energy, for example ionic conductors, are ideal candidates to observe this phenomenon. In fact, past work has observed ferroelectric transitions in ionic conductors [32–35].

5. Conclusions

We have demonstrated the possibility of polarization switching in epitaxially strained $H_{1/4}SNO$ between two symmetry-inequivalent states, which we term 'fraternal-twin ferroelectricity.' Specifically, the change in polarization derives from the added valence electron hopping from one NiO_6 to another, with the two structures not related by symmetry due to the underlying oxygen-octahedron rotation pattern. While this phenomenon is likely to be sensitive to temperature, growth conditions and other external factors it presents a new manner to construct metastable polar phases. In the age of materials design, these results pave the way for a new class of designed ferroelectrics.

Data availability statement

The data that support the findings of this study are openly available at the following URL/DOI: https://doi.org/10.24435/materialscloud:tg-8p.

Acknowledgments

We thank Shriram Ramanathan for useful discussions and acknowledge financial support from Office of Naval Research Grant N00014-17-1-2770.

ORCID iD

Michele Kotiuga https://orcid.org/0000-0002-2592-7342

References

[1] Rabe K M, Dawber M, Lichtensteiger C, Ahn C H and Triscone J M 2007 *Modern Physics of Ferroelectrics:Essential Background* (Springer) pp 1–30
[2] Jona F and Shriane G 1962 *Ferroelectric Crystals* (Dover)
[3] Horiuchi S and Tokura Y 2008 *Nat. Mater.* **7** 357–66
[4] Fennie C J and Rabe K M 2005 *Phys. Rev.* B **72** 100103(R)
[5] Benedek N A and Fennie C J 2011 *Phys. Rev. Lett.* **106** 107204
[6] Efremov D V, van den Brink J and Khomskii D I 2004 *Nat. Mater.* **3** 853–6
[7] Alexe M, Ziese M, Hesse D, Esquinazi P, Yamauchi K, Fukushima T, Picozzi S and Gösele U 2009 *Adv. Mater.* **21** 4452–5
[8] Young J, Lalkiya P and Rondinelli J M 2016 *J. Mater. Chem. C.* **4** 4016–27
[9] Park S Y, Kumar A and Rabe K M 2017 *Phys. Rev. Lett.* **118** 087602
[10] Shi J, Zhou Y and Ramanathan S 2014 *Nat. Commun.* **5** 4860
[11] Zhang Z *et al* 2018 *Nature* **553** 68–72
[12] Liu Q, Dalpian G M and Zunger A 2019 *Phys. Rev. Lett.* **122** 106403
[13] Kotiuga M and Rabe K M 2019 *Phys. Rev. Mater.* **3** 115002
[14] Perdew J P, Burke K and Ernzerhof M 1996 *Phys. Rev. Lett.* **77** 3865–8
[15] Perdew J P, Burke K and Ernzerhof M 1997 *Phys. Rev. Lett.* **78** 1396
[16] Kresse G and Furthmüller J 1996 *Phys. Rev.* B **54** 11169–86
[17] Kresse G and Joubert D 1999 *Phys. Rev.* B **59** 1758–75
[18] Blöchl P E 1994 *Phys. Rev.* B **50** 17953–79

[19] Liechtenstein A I, Anisimov V I and Zaanen J 1995 *Phys. Rev.* B **52** R5467
[20] Blöchl P E, Jepsen O and Andersen O K 1994 *Phys. Rev.* B **49** 16223–33
[21] Ong S P, Richards W D, Jain A, Hautier G, Kocher M, Cholia S, Gunter D, Chevrier V L, Persson K A and Ceder G 2013 *Comput. Mater. Sci.* **68** 314–9
[22] King-Smith R D and Vanderbilt D 1993 *Phys. Rev.* B **47** 1651–4
[23] Diéguez O, Rabe K M and Vanderbilt D 2005 *Phys. Rev.* B **72** 144101
[24] Kotiuga M and Rabe K M 2021 *Mater. Cloud Arch.* (https://doi.org/10.24435/materialscloud:tg-8p)
[25] Talirz L *et al* and 2020 *Sci. Data* **7** 299
[26] Qi Y and Rabe K M 2022 *Phys. Rev. B* **106** 125131
[27] Hyeon Lee S, Kim M, Ha S D, Lee J W, Ramanathan S and Tiwari S 2013 *Appl. Phys. Lett.* **102** 072102
[28] Zhou Y *et al* 2016 *Nature* **534** 231–4
[29] Kotiuga M *et al* 2019 *Proc. Natl Acad. Sci.* **116** 21992–7
[30] Zhang H-T *et al* 2020 *Nat. Commun.* **11** 2245
[31] Yuan Y *et al* 2023 arXiv:2311.12200
[32] Scott J F, Habbal F and Zvirgzds J A 1980 *J. Chem. Phys.* **72** 2760–2
[33] Baranov A I, Khiznichenko V P and Shuvalov L A 1989 *Ferroelectrics* **100** 135–41
[34] Stefanovich S Y, Mill B V and Butashin A V 1993 *Ferroelectrics* **144** 237–43
[35] Zhou S *et al* 2020 *Mater. Horiz.* **7** 263–74